Supporting information:

The simplest supramolecular helix

Felix Hanke, Chloe J. Pugh, Ellis F. Kay, Joshua B. Taylor, Stephen M. Todd, Craig M. Robertson, Benjamin J. Slater and Alexander Steiner**

Index:

Models of helical stacks of simple dumbbells

(as the 3D-printed model shown in Fig. 1 of main text)

The dumbbells of the model shown in Fig. 1 in the main text consist of two equal spheres of diameter *b* that are connected by a rod of diameter *a*, while *c* describes the distance between the centres of the spheres. At certain proportions *a* : *b* : *c* these simple shapes of $D_{\infty h}$ symmetry form stable helical stacks (if held together by gravity, the two dumbbells at the bottom must be supported to keep the stack upright; alternatively, dumbbells can be equipped with dipoles in the form of bar magnets that penetrate the rods through their midpoints). The 3D-printed model in Fig.1 features dimensions 1 : 3.070 : 5.432 which marks a maximal contact structure where every sphere touches six other spheres resulting in a tubular close-packed arrangement of spheres.

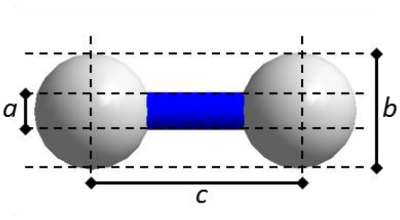

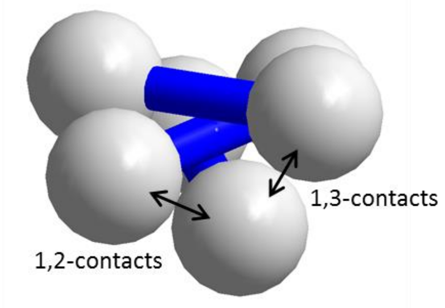

If dumbbells are stacked in a way that every rod is in contact with the rods of neighbouring dumbbells while spheres make contacts to spheres of nearest (1,2-contacts) and second nearest neighbours (1,3-contacts) such that every sphere is in contact with four other spheres, then all dumbbells are locked into position with fixed dihedral angles between them. Equation (S1) describes this condition, which applies within the boundaries $2 \leq b/a < 3.0703$:

$$c = \sqrt{\frac{1}{4}b^2 - a^2} + \sqrt{\frac{9}{4}b^2 - 3a^2} \qquad \textit{(S1)}$$

The graph in Fig. S1 shows *c* as a function of *b* (with *a* = 1). The point *b*/*a* = 2 marks the lower limit for 1,3-contacts to occur. It produces a maximum contact structure (with four 1,2-contacts and two-1,3 contacts) resulting in a non-helical stack with a dihedral angle between neighbouring dumbbells of 90°. Only when *b* is greater than 2×*a* competing length scales due to 1,3-contacts develop which will induce a helical twist. Marking the arrival of additional 1,4-contacts, a maximal contact structure is obtained again at *b*/*a* ≈ 3.0703 (with two 1,2 contacts, two 1,3-contacts and two-1,4 contacts), this time in helical form with a dihedral angle of 64.606° (equivalent to the model in Fig. S1 and in Fig. 1 of the main text). Beyond this point 1,4-contacts will take effect and the dependency of equation *(S1)* breaks down as other relationships will apply.

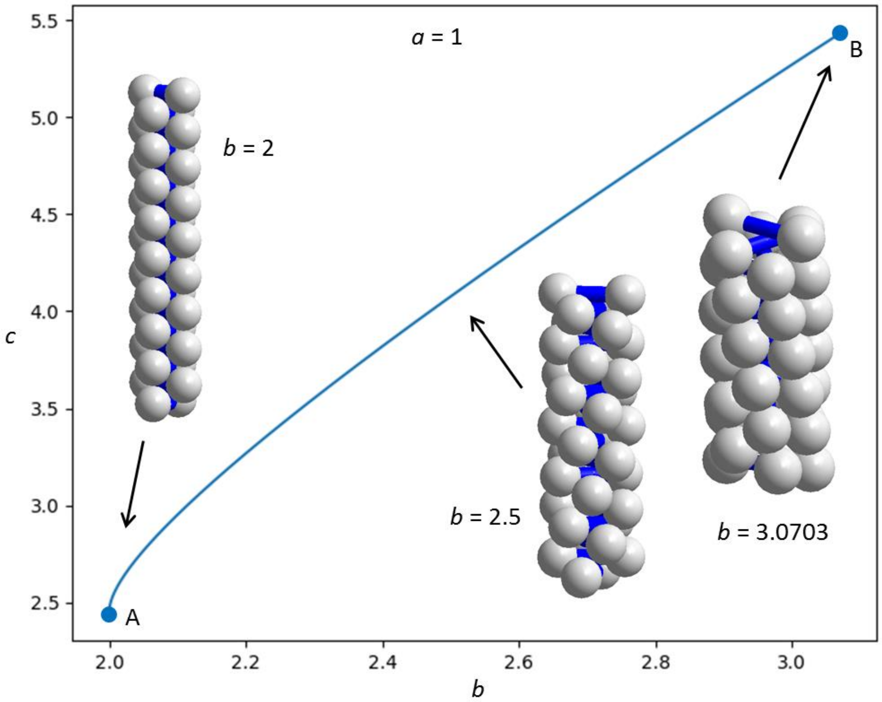

Fig. S1 The blue curve describes the helical stacks that show both 1,2-and 1,3-contacts according to equation *(S1)* . Point A marks the lower limit for 1,3-contacts, point B the lower limit for 1,4-contacts to occur.

It should be noted that the helix with $b/a \approx 3.0703$ is the first member of an infinite series of helical stacks of dumbbells that exhibit maximal contacts and thus form close packed tubular structures. These are closely related to the dense packings of spheres in cylinders.[S1,S2] Fig. S2 shows the first members including the non-helical structure with $b/a = 2$ alongside their corresponding "rolled-out" patterns. In the notation (l, m, n)[S1] l is the number of spheres that are in direct contact to form the shortest path around the cylinder starting and ending at the same sphere, while m and n mark the lengths the path takes along each of its two directions (as indicated by the blue arrows). The condition for stacks of dumbbells to form is satisfied when both $m/2$ and $n/2$ are integers that have no common divisor greater than 1 (otherwise the rods would intersect). Stacks with $m \neq n$ are helical as they lack reflection symmetry, while stack (4, 2, 2) is the only non-helical stack ($m = n$) in this series.

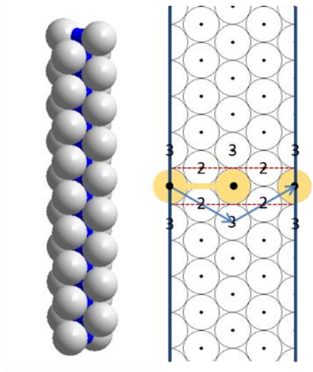

(4, 2, 2)

b = 2.0000, c = 2.4495, θ = 90.000°

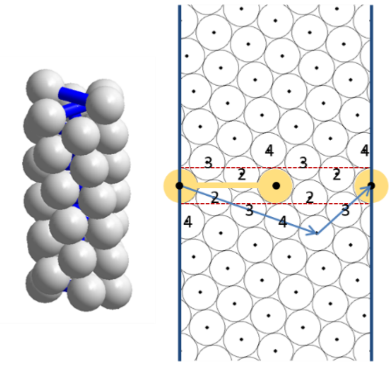

(6, 4, 2)

b = 3.0703, c = 5.4321, θ = 64.606°

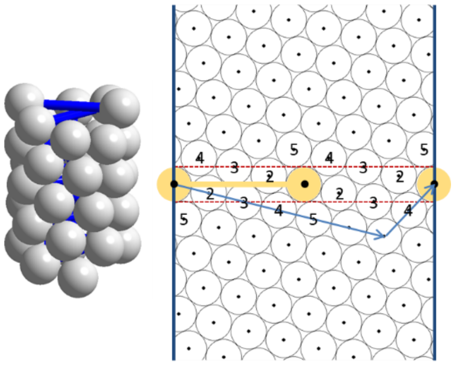

(8, 6, 2)

b = 4.1830, c = 9.8781, θ = 48.558°

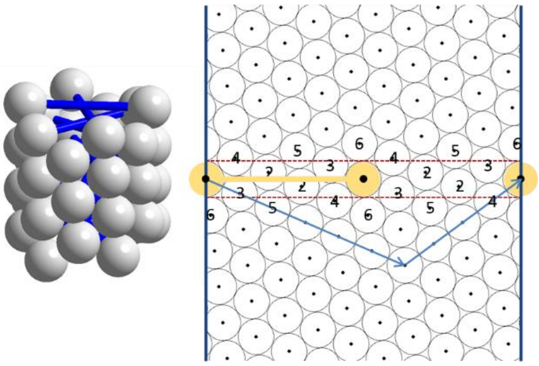

(10, 6, 4)

b = 5.0365, c = 14.2148, θ = 71.023°

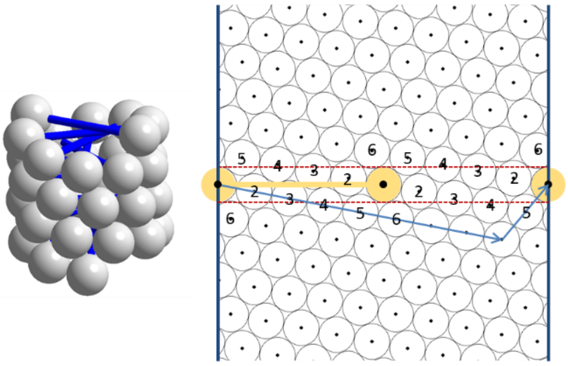

(10, 8, 2)

b = 5.3105, c = 15.7782, θ = 38.605°

Fig. S2 First five members of an infinite series of stacks of dumbbells (with a = 1) that exhibit maximal contacts (where every sphere is in direct contact with six others) alongside their "rolled-out" pattern. The spheres of one dumbbell are highlighted; numbers inside circles indicate i-th dumbbell along stack to illustrate 1,i contacts between spheres.

Global optimization of the modified dumbbell model

The globally optimized dumbbell model in Fig. 5 was adopted from Ref. S3. It consists of three Lennard-Jones beads arranged to reflect the C_s symmetry of the Et_2NH molecule. Two equivalent beads represent the ethyl groups, while the central bead represents the amide group and has a strong dipole moment attached to it, which is perpendicular to the plane formed by the three spheres. Varying the internal angle formed between the spheres leads to helical conformations over a wide range of angles and parameter sets. Here we present a full set of data for a range of internal angles with the following set of constant parameters.

A Lennard-Jones is applied pairwise between spheres *i* and *j*, $V_{ij}(r) = 4\varepsilon_{ij}\left[\left(\frac{\sigma_{ij}}{r}\right)^{12} - \left(\frac{\sigma_{ij}}{r}\right)^{6}\right]$, where $\varepsilon_{ij} = 1, \sigma_{11} = 1, \sigma_{22} = 0.46, \sigma_{12} = \sqrt{\sigma_{11}\sigma_{12}}$. The outer spheres are both labelled 1, the inner sphere has index 2 for each particle. The dipole moment associated with the inner sphere has dimensionless units 5.

The global optimizations are run for 10000 steps with the basin hopping algorithm implemented by Wales and Doyle.[S4] The calculations shown below are for 10 particles, test calculations with up to 20 particles in a given system have shown that these calculations are converged in that they consistently leading to the same minimum structure motifs.

Fig.S3 presents the results from runs with different internal angles of the dumbbell potential, which shows no helix for internal angles of 180°, helix global minima for internal angles between 180° and around 130°, and different clustering at 120° internal angle. These global optimizations demonstrate that simple model potentials with the same coarse grained features and symmetry as the Et_2NH molecule do preferentially form helical structures.

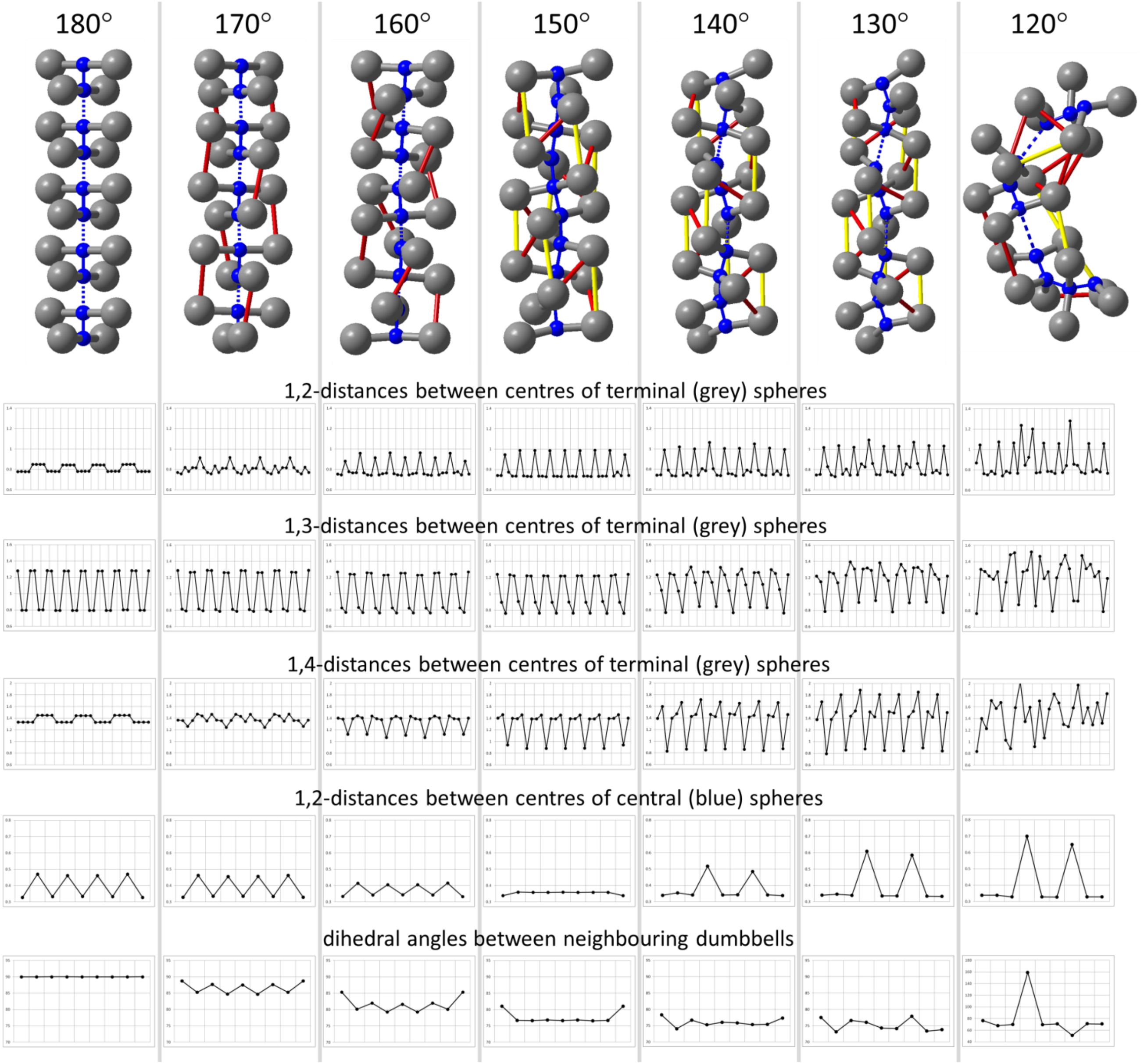

Fig. S3 Global minimum structures and interparticle distances for three-body dumbbells from runs with different internal angles of the dumbbell potential. Shortest 1-3 and 1-4 interactions between terminal (grey) spheres are shown in red and yellow respectively, while dashed lines between show longer interactions between central spheres. Linear dumbbells with an internal angle of α=180° stack alternatingly without forming a helix, while bent dumbbells with internal angles between 180° and 120° form helical stacks. At α=170° the helical structure is already apparent, while at α=150° it is most uniform. At α=120° the helical symmetry disappears and the original stack collapses into a cluster.

Molecular dynamics sampling of tetramer conformers

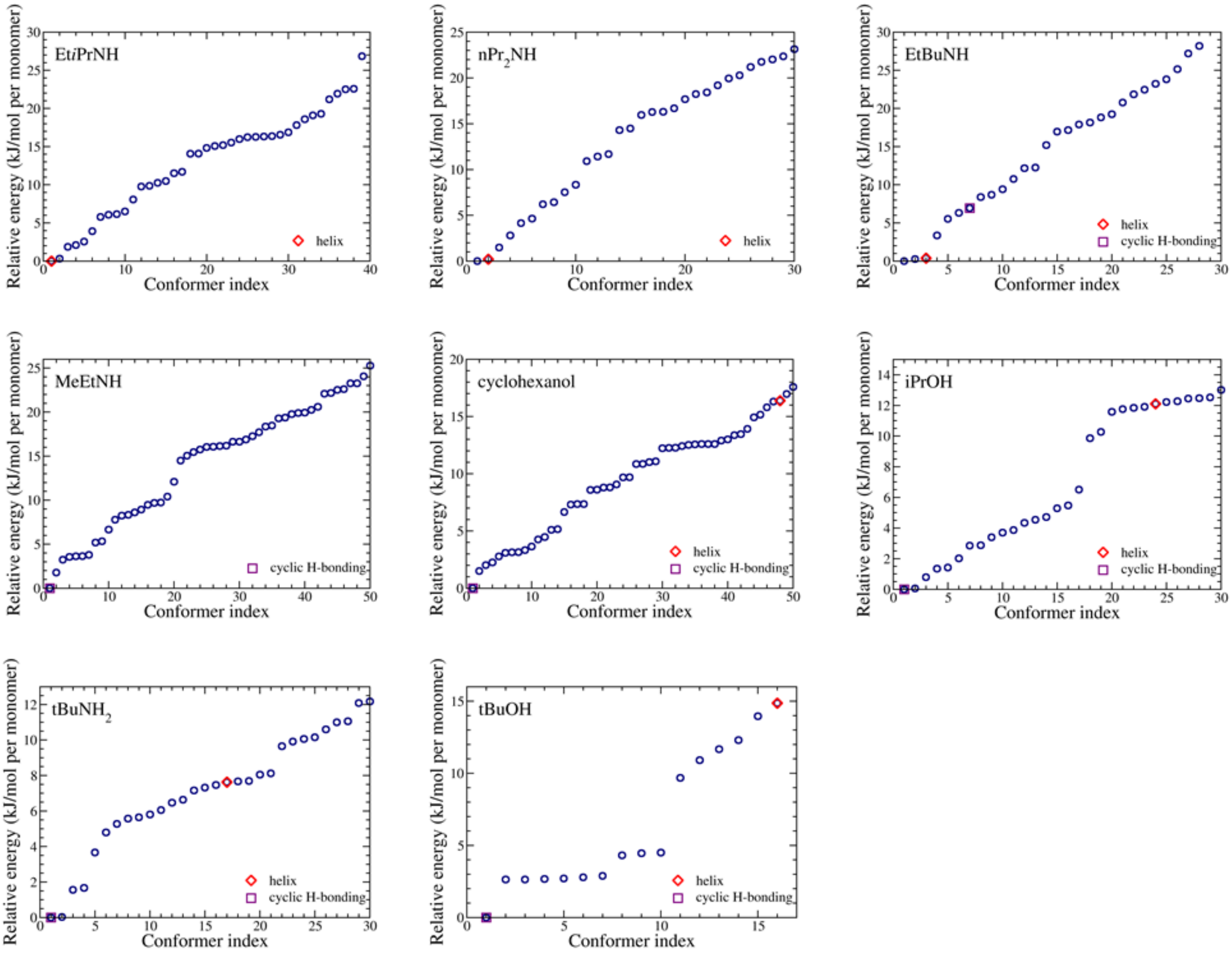

Fig. S4 Additional results similar to Fig 4 in the manuscript to confirm that the helical behaviour observed in the dialkylamine tetramers is unique to certain sizes of this particular class of molecules. Shown are results for helical supramolecular assemblies (Et*i*PrNH and *n*Pr_2NH which did not show any cyclic tetramers; EtBuNH), MeEtNH for which the sampling did not return any helices but which instead stabilizes into a cyclic tetramer, and a number of other molecules which show helical behaviour in a number of polymorphs but in the gas phase are all outcompeted by cyclic conformers (*i*PrOH, *t*$BuNH_2$, *t*BuOH, cyclohexanol). Note that most of the conformers found for *t*BuOH are equivalent cyclically bound systems, of which only one is shown.

Crystallisation and X-ray structure determination

Samples of dialkylamines were purchased from Sigma-Aldrich and used without further purification. All compounds are liquid at room temperature. They were crystallized in-situ using the zone-melting technique described by Boese and Nussbaumer.[S5] In a typical experiment, the sample was filled into a capillary, mounted onto the diffractometer (Bruker Apex II), flash-frozen at 100 K and then warmed to about 20 degrees below its melting point. It was then subjected to successive heating scans along the capillary using an infrared laser until sufficiently large single crystals had formed.

The phase behaviour of the solids was monitored on the diffractometer by cycling the temperature of the sample starting from the liquid phase down to 100 K and back to the melt. Melting occurred at 185 K (MeEtNH), 223 K (Et_2NH), 210 K (Pr_2NH), 195 K (EtBuNH), 211 K (Bu_2NH), 276 K (Hx_2NH), 198 K (Et*i*PrNH), 178 K (*i*Pr_2NH) and 203 K (*i*Bu_2NH). With the exception of diethylamine all compounds exhibited uniform solid phases above 100 K. Et_2NH showed a solid-solid phase change at 148 K in a single-crystal-to-single-crystal transformation. A single crystal of its low temperature phase was obtained by slowly cooling a single crystal of the high temperature phase through the solid-solid phase transition.

Single crystal X-ray data were recorded at 100K, except for the high temperature phase of Et_2NH, which was measured at 160 K. The experimental setup required that the capillary was always kept in a vertical alignment, which limited the coverage of reflections. All structures were solved with Direct Methods and refined against F^2 using full-matrix least-squares (SHELXL-2014).[S6,S7] Multi-domain non-merohedral twin refinements were carried out for Et_2NH-HT and MePrNH. C and N atoms were refined anisotropically, H atoms isoptropically. The positional parameters of N-bonded H-atoms were refined freely, while C-bonded H-atoms were fixed in geometrical positions (one parameter was used for the rotation of methyl groups). Crystal structures of Et_2NH-LT, Et_2NH-HT, iPr_2NH and iBu_2NH showed disorder of H-atoms in NH...N bridges. All other compounds showed ordered hydrogen positions.

CCDC 1826573 (Bu_2NH), 1826574 (Hx_2NH), 1826575 (Et_2NH-HT), 1826576 (*i*Bu_2NH), 1826577 (*i*Pr_2NH), 1826578 (Et*i*PrNH), 1826579 (MeEtNH), 1826580 (Et_2NH-LT), 1826581 (MePrNH), 1826582 (EtBuNH), 1826583 (Pr_2NH) contain the supplementary crystallographic data for this paper. These data can be obtained free of charge from The Cambridge Crystallographic Data Centre.

Table S1 Crystal data of dialkylamines that form helices in the solid state.

	Et$_2$NH-LT	Et$_2$NH-HT	Pr$_2$NH	EtBuNH	Et*i*PrNH
formula	$C_4H_{11}N$	$C_4H_{11}N$	$C_6H_{15}N$	$C_6H_{15}N$	$C_5H_{13}N$
MW	73.14	73.14	101.19	101.19	87.16
spacegroup	$P2_1$/n	$C2$/c	$P2_1$/c	Cc	$P2_1$/n
a/Å	7.989(2)	8.0789(19)	8.158(2)	14.348(4)	8.933(18)
b/Å	15.320(5)	15.538(4)	10.492(3)	8.940(3)	9.062(19)
c/Å	13.213(4)	13.319(3)	26.090(7)	17.768(6)	15.56(3)
α/°	90	90	90	90	90
β/°	96.290(5)	98.065(4)	90.156(4)	105.637(4)	99.55(3)
γ/°	90	90	90	90	90
V/Å^3	1607.5(8)	1655.5(7)	2233.3(10)	2194.8(11)	1242(4)
Z	12	12	12	12	8
T/K	100(2)	160(2)	100(2)	100(2)	100(2)
d/g cm^{-3}	0.907	0.88	0.903	0.919	0.932
μ/mm^{-1}	0.054	0.053	0.053	0.054	0.055
R(int)	0.030	0.021	0.035	0.035	0.077
θ(max)	26.40	26.42	26.46	26.34	25.52
coverage	0.98	0.85	0.89	0.90	0.91
refl(unique)	3200	1408	3999	3192	2086
refl(>2σ(I))	2732	1152	3148	3012	1223
parameter	162	85	208	209	123
$R1$(>2σ(I))	0.050	0.043	0.047	0.036	0.083
$wR2$(all)	0.122	0.115	0.122	0.095	0.253

Table S2 Crystal data of dialkylamines that form non-helical structures.

	Bu_2NH	Hx_2NH	MeEtNH	MePrNH	$i Pr_2NH$	$i Bu_2NH$
formula	$C_8H_{19}N$	$C_{12}H_{27}N$	C_3H_9N	$C_4H_{11}N$	$C_6H_{15}N$	$C_8H_{19}N$
MW	129.24	185.34	59.11	73.14	101.19	129.24
spacegroup	*P*bcm	*P*bcm	$P2_1$/n	*C*2/c	*C*2/c	*C*2/c
a/Å	4.8201(15)	4.856(4)	7.761(5)	15.168(15)	14.527(8)	17.442(11)
b/Å	7.003(2)	7.056(6)	16.084(13)	8.902(8)	7.293(4)	11.612(8)
c/Å	26.028(8)	36.24(3)	14.231(12)	15.176(15)	14.148(6)	18.375(12)
α/°	90	90	90	90	90	90
β/°	90	90	99.851(10)	90.67(2)	104.794(11)	90.080(15)
γ/°	90	90	90	90	90	90
V/Å^3	878.5(5)	1241.9(19)	1750(2)	2049(3)	1449.4(12)	3722(4)
Z	4	4	16	16	8	16
T/K	100(2)	100(2)	100(2)	100(2)	100(2)	100(2)
d/g cm^{-3}	0.977	0.991	0.897	0.948	0.927	0.923
μ/mm^{-1}	0.056	0.056	0.055	0.057	0.054	0.053
R(int)	0.039	0.053	0.129	0.045	0.034	0.061
θ(max)	26.43	26.43	24.68	25.51	26.40	26.59
coverage	0.96	0.95	0.77	0.87	0.93	0.77
refl(unique)	874	1216	2292	2659	1359	2879
refl($>2\sigma$(I))	723	595	1428	1817	1108	1972
parameter	47	65	169	104	76	185
$R1$($>2\sigma(I)$)	0.050	0.048	0.073	0.089	0.038	0.076
$wR2$(all)	0.181	0.142	0.181	0.292	0.093	0.207

Table S3 Structural parameters of helices of dialkylamines

	Et_2NH-LT	Et_2NH-HT	Pr_2NH	EtBuNH	Et*i*PrNH
Z'	3	1.5	3	3	2
Molecules per pitch	3	3	3	3	4
N...N (Å)	3.179(2) 3.180(2) 3.275(2)	3.251(2) 3.225(3)	3.204(2) 3.205(2) 3.285(2)	3.391(3) 3.303(4) 3.309(3)	3.477(7) 3.505(7)
N...N...N (°)	130.0 115.7 121.3	120.2 123.3	119.2 120.0 134.6	120.4 122.6 132.0	115.1 113.7
N...N...N...N (°)	98.7 110.5 122.9	106.8 112.2	102.9 104.6 127.4	103.5 108.1 123.0	50.6 82.4
pitch length (Å)	7.989(2) [a]	8.079(2) [a]	8.158(2) [a]	8.453(3) [b]	9.062(19) [c]
θ (°) [d]	17.9 19.3 20.8	16.9 20.3	14.8 17.8 18.8	17.1 23.2 23.5	36.1 42.7

[a] equal to unit cell parameter *a*; [b] equal to $(a^2 + b^2)^{½} / 2$; [c] equal to *b*

[d] inclination of molecule with respect to helical axis (measured from C2 positions):

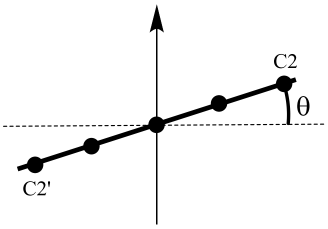

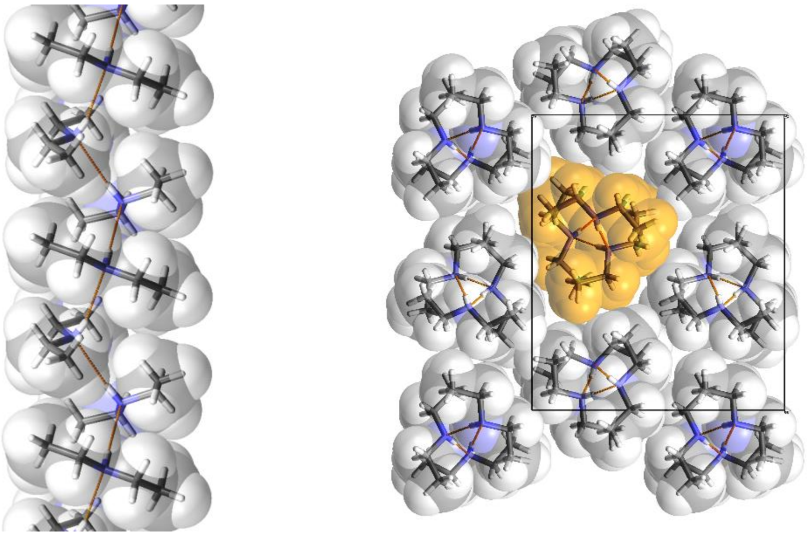

Et_2NH-LT

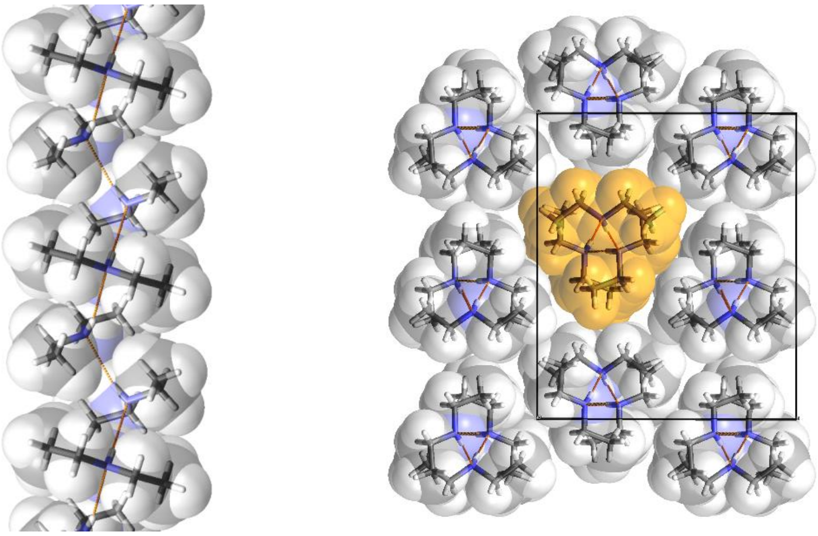

Et_2NH-HT

Fig. S5 Crystal structures of the low and high-temperature phases of Et_2NH. Diagrams on the left show helical strands; diagrams on the right depict the packing of helices parallel to [1 0 0]. One strand is highlighted to illustrate the pseudo-hexagonal packing of helical strands. The transition from the HT to the LT-phase preserves the helix, but reduces the symmetry of the structure. In Et_2NH-LT the three molecules that make up its pitch are symmetry-independent ($Z' = 3$). The helix of Et_2NH-HT has 2-fold rotation symmetry perpendicular to its helical axis ($Z' = 1.5$). In both structures the H-atoms of H-bonds are disordered over two positions (only one is shown here for clarity).

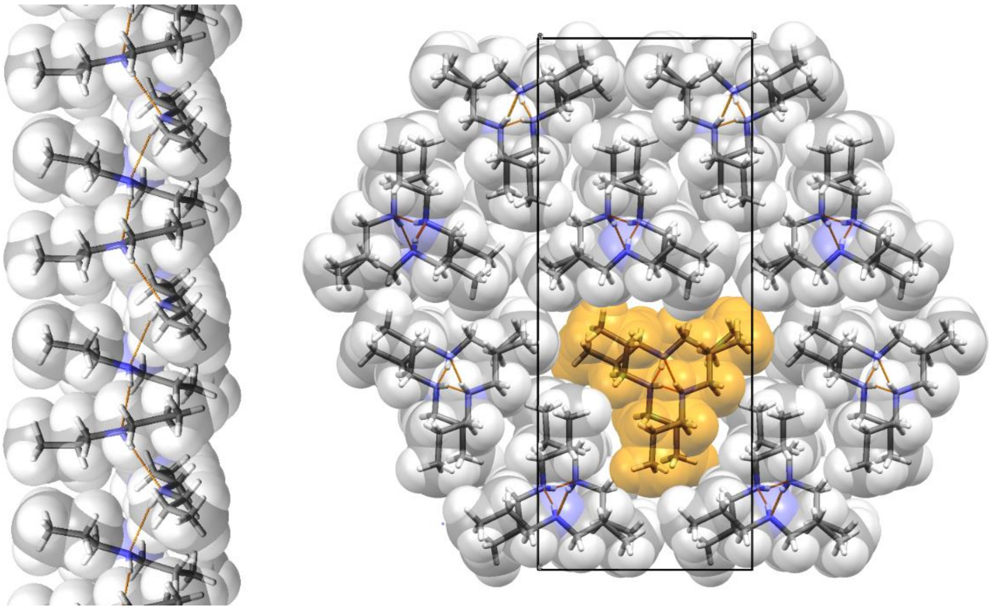

Pr_2NH

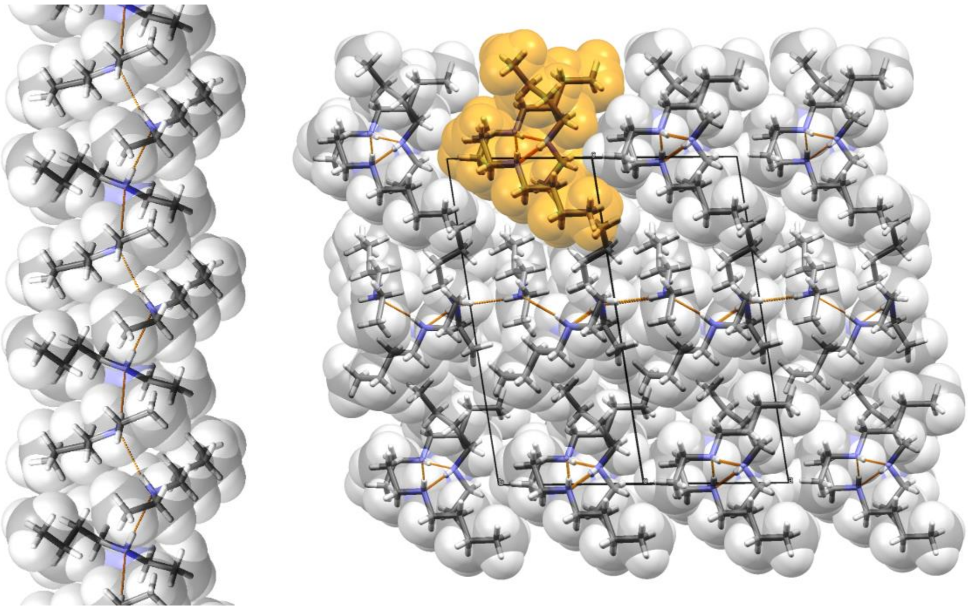

EtBuNH

Fig. S6 Crystal structures of Pr_2NH and EtBuNH. Diagrams on the left show helical strands; diagrams on the right depict the crystal packing: Helices of Pr_2NH run parallel to [1 0 0], while those of EtBuNH pack in alternating layers in which helices run in a crisscrossing pattern along directions [1 1 0] and [1 ¬1 0]. This arrangement may be effected by the asymmetric molecular shape of EtBuNH, which creates less compact helical columns due to its extending butyl groups (one strand is highlighted illustrating the more awkward shape of the helical columns). Crystals of Pr_2NH and EtBuNH contain three molecules per asymmetric unit ($Z' = 3$) that make up one helical pitch. Both crystal structures contain ordered H-bonds.

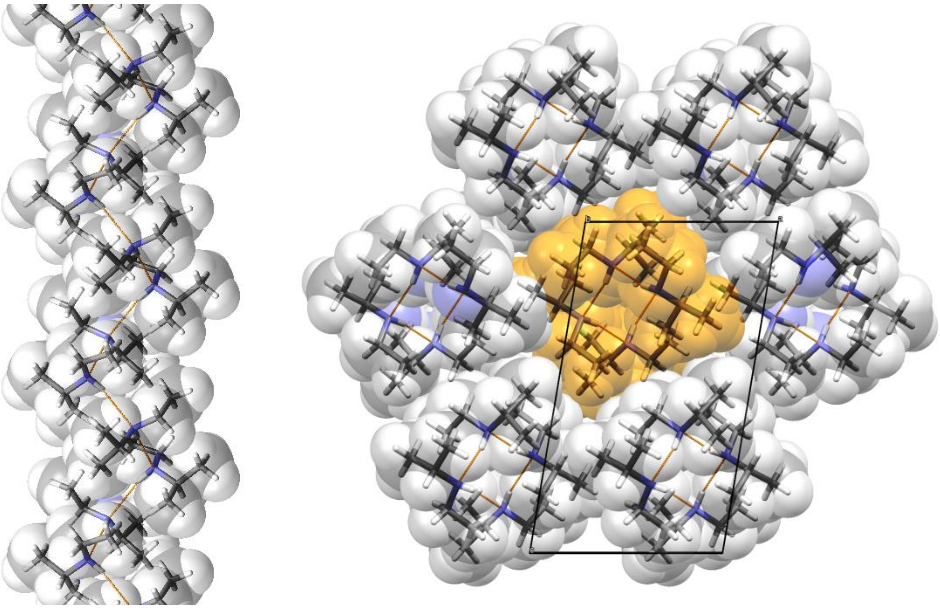

Et*i*PrNH

Fig. S7 Crystal structure of Et*i*PrNH. The diagram on the left shows one helical strand; the diagram on the right depicts the crystal packing. The helix of Et*i*PrNH runs parallel to [0 1 0]; it comprises four molecules per pitch, two of which are symmetry-independent, and contains ordered H-bonds.

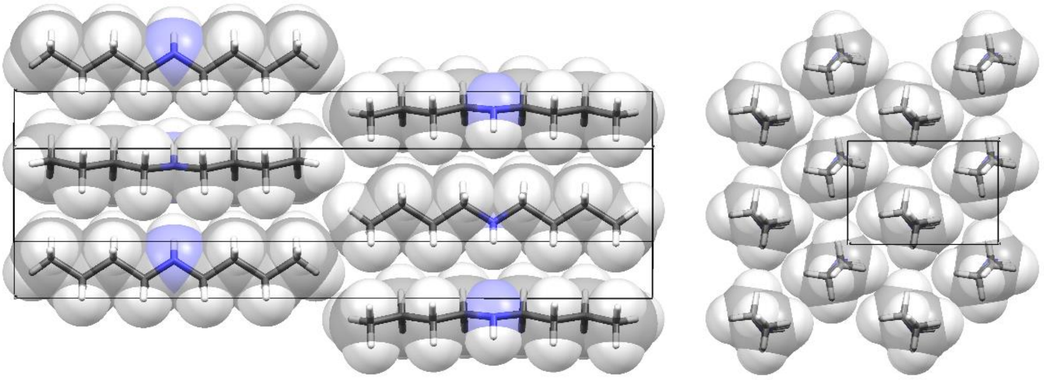

Bu_2NH

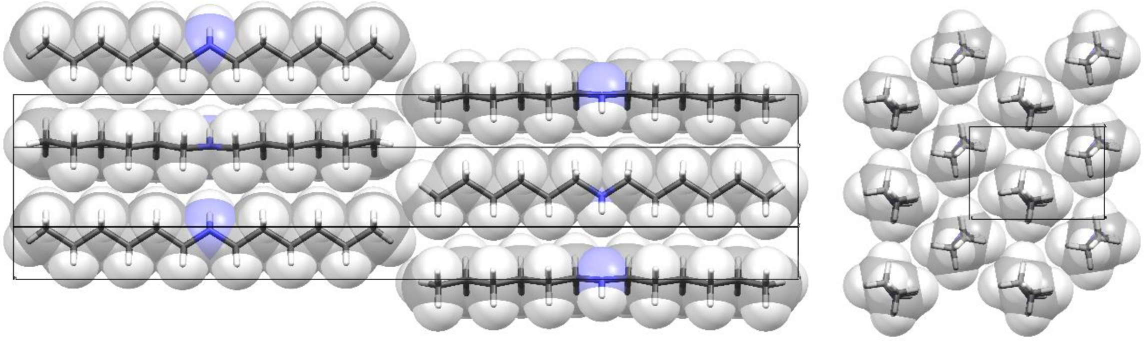

Hx_2NH

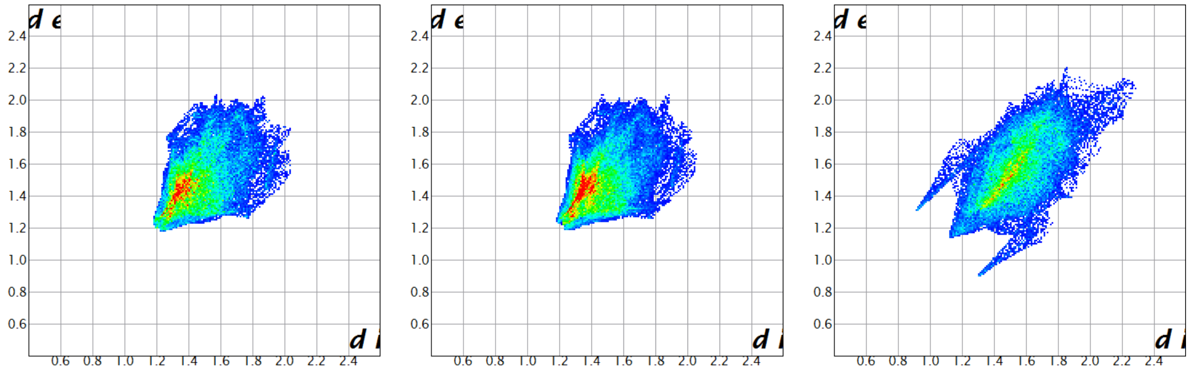

Bu_2NH Hx_2NH Pr_2NH

Fig. S8 Top: Packing diagrams of crystal structures of Bu_2NH and Hx_2NH illustrating the parallel packing typical to that of linear alkanes. Bottom: The fingerprint plots of Hirshfeld surfaces [S8] indicate the absence of hydrogen bonding in crystals of Bu_2NH and Hx_2NH. Short intermolecular N...H contacts would appear in the form of spikes along the wings as shown for the H-bonded structure of Pr_2NH. This indicates that the parallel packing becomes more efficient with longer alkyl groups even though it cannot accommodate hydrogen bonding.

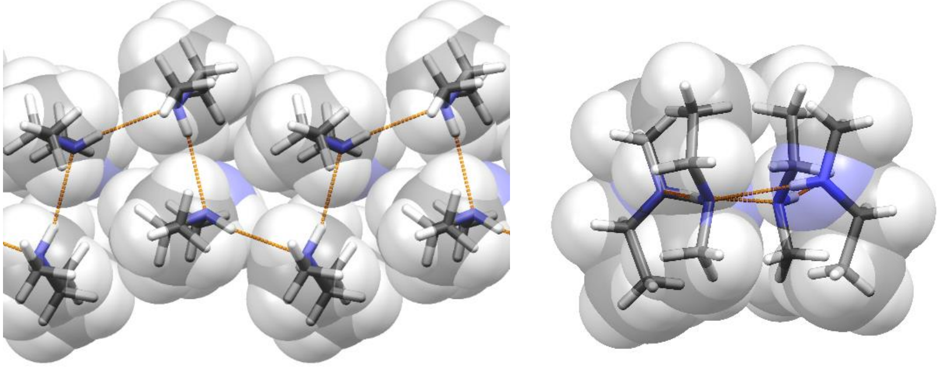

MeEtNH

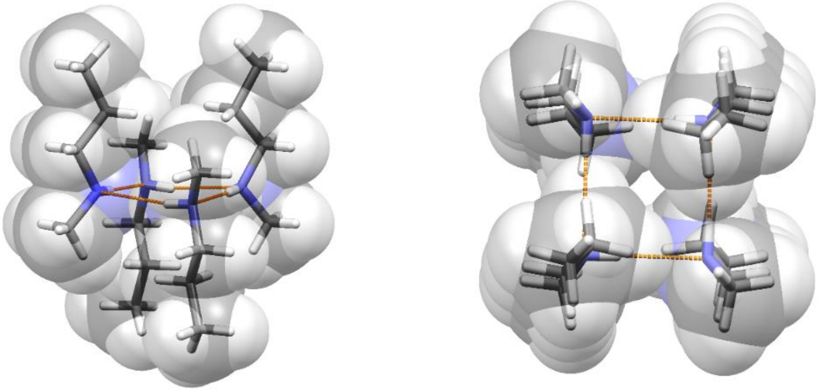

MePrNH

Fig. S9 Crystal structures of methyl derivatives MeEtNH and MePrNH. In contrast to helical arrangements, the molecules are aligned parallel to each other as the methyl group is too small to induce a twist between two H-bonded molecules (see also Fig. S10). Top: Two views of the crinkled chain of MeEtNH. The chain contains four independent molecules (Z' = 4). N...N distances in H-bonds of MeEtNH: 3.209(4), 3.290(4), 3.242(4) and 3.291(4) Å. Bottom: Two views of the tetramer of MePrNH. The tetramer has a crystallographic 2-fold rotation axis and contains two independent molecules. N...N distances in H-bonds of MePrNH: 3.224(6) and 3.329(6) Å. Both structures contain ordered hydrogen bonds.

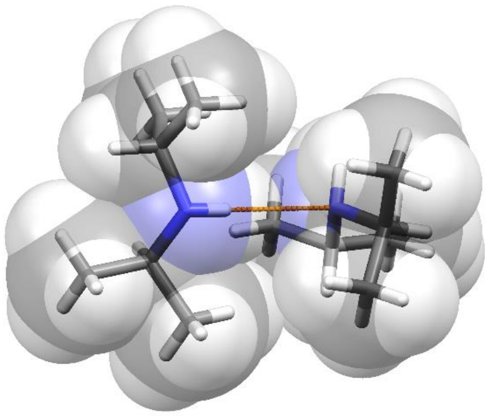

iPr_2NH

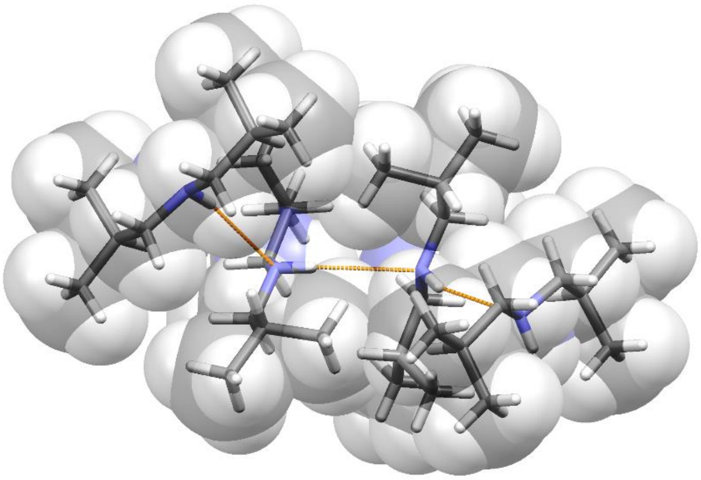

iBu_2NH

Fig. S10 Crystal structures of branched derivatives *i*Pr_2NH (dimer) and *i*Bu_2NH (tetramer). The steric bulk of two branched alkyl groups may prevent the formation of longer chains. Both the dimer of *i*Pr_2NH and the tetramer *i*Bu_2NH are located on a 2-fold rotation axis. As a result, the H-atoms of H-bonds are disordered over two positions.

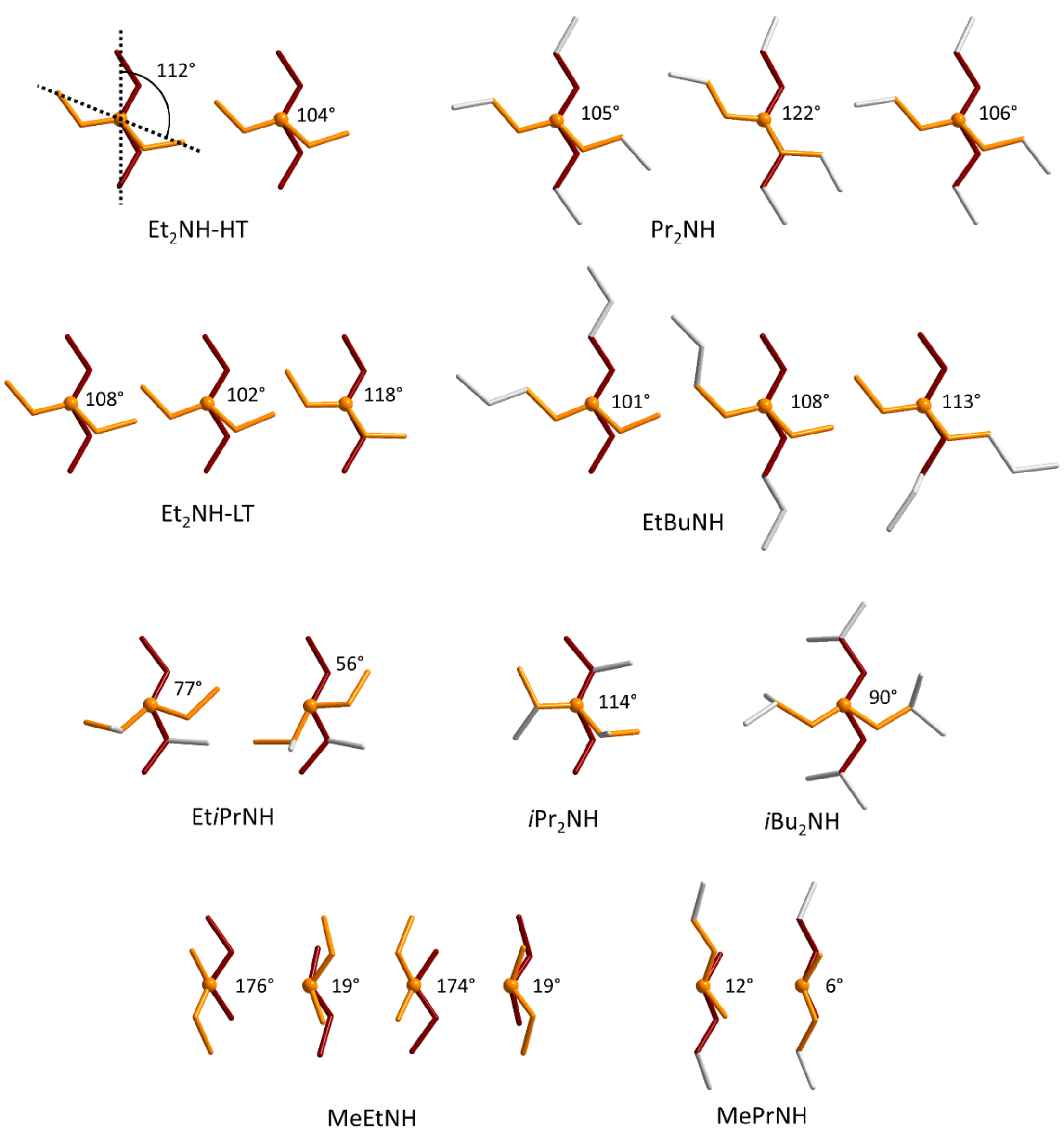

Fig. S11 Schematic representation of H-bonded pairs of molecules in crystal structures (this includes all symmetrically independent pairs of this study) viewed along their H-bonds. It displays the dihedral angle at which the central CCNCC backbones of the two molecules twist against each other (highlighted in orange and red). It shows that pairs with alkyl groups larger than methyl must twist away from a parallel alignment to form hydrogen bonding. Those that form helices with three molecules per pitch (Et_2NH, Pr_2NH and EtBuNH) show very similar angles. Methyl derivatives, on the other hand, are aligned in parallel with dihedral angles close to either 0° or 180°. This chart also shows that the linear, all anti-conformation of the CCNCC-units is maintained in all crystal structures of this study (one butyl group of EtBuNH deviates from linearity, but this effects only the outer part of the chain).

References

S1 A. Mughal, H. K. Chan, D. Weaire, S. Hutzler, *Phys. Rev. E,* 2012, **85**, 051305.

S2 L. Fu, W. Steinhardt, H. Zhao, J. E. S. Socolar, P. Charbonneau, *Soft Matter,* 2016 ,**12** , 2505.

S3 D. Chakrabarti, S. N. Fejer, D. J. Wales, *Proc. Natl. Acad. Sci.,* 2009, **106**, 20164.

S4 D. J. Wales, J. P. K. Doyle, *J. Phys. Chem. A,* 1997, **101**, 5111.

S5 R. Boese, M. Nussbaumer, *In Situ Crystallisation Techniques*, Oxford University Press, 1994.

S6 G. M. Sheldrick, *Acta Crystallogr., Sect. A,* 2008, **64**, 112.

S7 G. M. Sheldrick, *Acta Crystallogr, Sect. C,* 2015, **71**, 3.

S8 M. A. Spackman, J. J. McKinnon, *CrystEngComm,* 2002, **4**, 378.